

Dynamics of Spinning Three-Body Gravitational Systems using the Post-Newtonian
Approximation

Paul Argyle

A senior thesis submitted to the faculty of
Brigham Young University
In partial fulfillment of the requirements for the degree of

Bachelor of Science

David Neilsen, Advisor

Department of Physics and Astronomy

Brigham Young University

April 2022

Copyright © 2022 Paul Argyle

All Rights Reserved

ABSTRACT

Dynamics of Spinning Three-Body Gravitational Systems using the Post-Newtonian Approximation

Paul Argyle

Department of Physics and Astronomy

Bachelor of Science

We use the post-Newtonian approximation of general relativity to study three-body systems composed of pulsars and rotating black holes. We numerically solve the post-Newtonian equations of motion to two and a half order with the inclusion of spin coupling terms to leading order. We study the effects of spin on the Kozai mechanism. Spin coupling can alter the frequency of the Kozai mechanism and introduce new patterns of oscillations in compact systems. The amplitude and period of Kozai oscillations decrease with separation distance when the objects are sufficiently close that relativistic effects dominate. Simulations show spin effects can alter the merge time of binary black holes. We calculate gravitational waves produced by three-body systems.

Keywords: post-Newtonian, three-body, Kozai mechanism, black holes, general relativity

Acknowledgments

This research was supported by the department of Physics and Astronomy at Brigham Young University. I would like to thank Professor David Neilsen for mentoring me.

Table of Contents

Table of Contents.....	v
List of Figures.....	vii
List of Tables.....	viii
1 Introduction	9
1.1 <i>The Three-Body Problem</i>	9
1.2 <i>Kozai Mechanism</i>	10
1.3 <i>Spin Coupling in General Relativity</i>	11
1.4 <i>Three-Body Effects on Black Hole Mergers</i>	11
1.5 <i>Overview</i>	13
2 Methods	14
2.1 <i>Post-Newtonian Approximation</i>	14
2.2 <i>Initial Conditions and Parameters</i>	15
2.3 <i>Numerical Methods and Tests</i>	17
2.3.1 <i>Integration Method and Units</i>	17
2.3.2 <i>Testing First and Second Order Post-Newtonian Equations</i>	17
2.3.3 <i>Testing 2.5 Order and Spin Coupling Post-Newtonian Equations</i>	18
2.4 <i>Gravitational Waves</i>	20
2.4.1 <i>Quadrupole Theory of Gravitational Waves</i>	20
2.4.2 <i>Numeric Implementation and Testing</i>	22
3 Results and Conclusions.....	24

3.1	<i>Spin Angular Momentum Coupling</i>	24
3.1.1	<i>Spin Effects on Kozai Mechanism</i>	24
3.1.2	<i>Evolution of Spin Angular Momenta</i>	27
3.2	<i>Comparing Post-Newtonian Orders</i>	29
3.3	<i>Radial Dependence</i>	30
3.4	<i>Spin Effects on Merge Times</i>	31
3.5	<i>Gravitational Wave Simulations</i>	33
3.6	<i>Conclusion</i>	36
Appendix A		38
	<i>Post Newtonian Hamiltonian</i>	38
Appendix B		42
	<i>Orbital Elements Definitions</i>	42
	<i>Conversion from Orbital Elements to Cartesian Coordinates</i>	43
	<i>Converting Cartesian Coordinates to Orbital Elements</i>	45
Index		47
Bibliography		48

List of Figures

Figure 1.1 Hierarchal triplet system.....	10
Figure 2.1 Simulated binary inspiral.....	19
Figure 2.2. Eccentric two-body simulation of rotating black holes	20
Figure 2.3. Gravitational waves from circular orbit.....	23
Figure 3.1. Spin effects on Kozai mechanism	26
Figure 3.2. Time evolution of spin angular momenta.....	28
Figure 3.3. Kozai mechanism at different post-Newtonian orders	29
Figure 3.4. Amplitude and period of Kozai osscitations vs. separation distance	30
Figure 3.5. Merge simulation in PNB2 model.....	32
Figure 3.6. Merge simulation in PNB1 model.....	33
Figure 3.7. Gravitational waves at 5000 km in PNN model.....	34
Figure 3.8. Gravitational waves just before merge event in PNN model	35
Figure B.1. Orbital elements.....	43

List of Tables

Table 2.1. Simulation Parameters16

1 Introduction

1.1 The Three-Body Problem

The gravitational three-body problem consists of solving for the motion of three masses under the influence of their mutual gravitational interaction. The three-body problem has no general analytic solution in terms of elementary functions, and in general must be solved numerically [1]. Physicists have been studying the gravitational three-body problem since the time of Newton. Most of these studies used Newton's law of Gravitation. The Newtonian gravitational three-body problem is known to be chaotic and exhibits a variety of nonlinear effects. Newton's law of gravitation is accurate for systems with weak gravity but breaks down for systems with strong gravity. In strong gravity systems, Einstein's theory of general relativity must be used.

There are several important applications of the relativistic gravitational three-body problem. One example is triplet systems of pulsars and white dwarfs. Radio signals from a pulsar orbiting two white dwarfs were observed by an international group of astronomers in 2014 [2]. Comparing observations from such systems with predictions of general relativity could be a new test of general relativity. Three-body interactions can also cause binary black holes to merge faster [3,4]. One way this can occur is through a three-body orbital resonance known as the Kozai mechanism. We study this three-body interaction numerically. Instead of solving the full Einstein equations directly, we obtain equations of motion by adding perturbations to the Newtonian Hamiltonian in a method called post-Newtonian approximation.

1.2 Kozai Mechanism

The Kozai Mechanism is an orbital resonance occurring in hierarchical triplet systems. Hierarchical triplet systems consist of two close orbiting masses with a third mass orbiting these objects from much farther away. A hierarchal triplet system is depicted in Fig. 1.1. The orbit consisting of the two close masses is called the inner binary. The tertiary mass and the center of mass of the inner binary comprise the outer binary. The minor radius of the outer binary is much larger than the radius of the inner binary $a_{out} \gg a_{in}$. The outer object perturbs the inner orbit over the course of several orbital periods. This causes oscillations between the eccentricity of the inner binary and relative inclination between the orbits known as the Kozai mechanism. The Kozai mechanism has been studied using Newtonian mechanics and various approximations of general relativity [5]. We study the Kozai mechanism using the post-Newtonian approximation, including spin coupling effects.

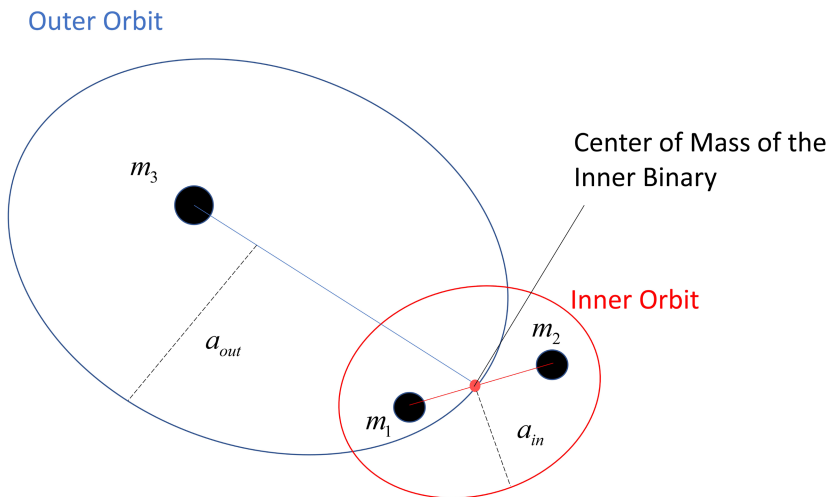


Fig 1.1 Depiction of a hierarchical three-body system. The inner binary is composed of two closely orbiting masses m_1 and m_2 . The outer binary consists of a tertiary mass m_3 and the center of mass of the inner binary. The minor radius of the outer binary is much larger than the radius of the inner binary $a_{out} \gg a_{in}$.

1.3 Spin Coupling in General Relativity

The gravitational field in general relativity couples to all forms of energy including an object's rotational kinetic energy. A rotating mass will drag the spacetime around it. In 1963 Roy Kerr discovered an exact solution to the Einstein equations for the case of an axially symmetric rotating black hole. The Kerr solution shows there is a fundamental limit on a black hole's spin angular momentum¹. In units where $G = 1$ and $c = 1$ this maximum value is the black hole's mass squared $S_{\text{Max}} = M^2$. Radio and optical observations have found evidence for black holes with spin angular momentum greater than 80% this maximum value [6].

In this work we are interested in studying spin effects on orbital dynamics. Spin angular momentum can affect orbital mechanics in several ways. The objects' spin angular momenta will couple with their orbital angular momentum. The spin angular momenta of different objects will couple. Deformation in the objects themselves due to their spin will also affect the gravitational field. We incorporate all these effects in our three-body simulations.

1.4 Three-Body Effects on Black Hole Mergers

In addition to spin effects, gravitational waves can play a role in systems with strong gravity. Gravitational waves are transverse waves in spacetime that propagate at the speed of

¹ The Kerr solution predicts that black holes with spin angular momenta $S > M^2$ will have a space-time singularity not enclosed by an event horizon. This is a naked singularity. In what is often referred to as the "cosmic censorship hypothesis" this is believed to be impossible.

light. They are produced by accelerating masses. Gravitational waves can cause black hole binaries to merge. As black holes in a close binary orbit about their center of mass they will lose energy to gravitational waves. This causes the separation distance to decrease and the orbital velocity to increase. Eventually this process can cause the binary to merge. This can take millions to billions of years depending on the initial separation and masses of the binary [7].

The waveforms from many of these events have been detected by LIGO (Laser Interferometer Gravitational Wave Observatory). By comparing these measurements with predictions from general relativity, the masses of the merging black holes can be deduced. Many of the black holes observed by LIGO have masses greater than $65 M_{\odot}$ with the most massive black hole observed to date weighing in at about $142 M_{\odot}$. Stellar evolution models suggest that black holes with masses greater than about $65 M_{\odot}$ should not be able to form from the collapse of a star. It is predicted that near the end of their life, supermassive stars with masses greater than $65 M_{\odot}$ will undergo a pair-instability supernova. In a pair-instability supernova, energetic atomic nuclei and gamma rays produce electrons and positrons that temporarily reduce the internal pressure supporting the star from gravitational collapse. This leads to a partial collapse and subsequent thermonuclear explosion that blows the star apart without leaving any stellar remnant behind. Thus, to align our understanding of stellar evolution with LIGO data, researchers have explored alternatives to stellar collapse to explain these higher mass black holes.

The leading explanation for the formation of black holes with masses greater than $65 M_{\odot}$ is formation through dynamical merger events. However, there could be a potential problem with this explanation. The time it takes an isolated binary black hole system to merge has been studied

[7]. Given the time it takes for isolated black hole binaries to merge and the current age of the universe, estimates have shown that it is unlikely LIGO would have observed so many black holes that are too massive to form through stellar evolution [8,9,10]. To provide an explanation, researchers have explored the effect multibody interactions have on the time it takes black holes to merge. It has been shown that the Kozai mechanism can decrease this merge time significantly [3,4]. However, this analysis was limited to systems in which the objects were not spinning. We do three-body simulations to study any potential effects spin coupling has on the Kozai mechanism and merge times of binary black holes.

1.5 Overview

In this work, we used the post-Newtonian approximation to study three-body systems composed of black holes and neutron stars. We numerically solve the post-Newtonian equations of motion to two and a half order with the inclusion of spin coupling terms to leading order. We analyze the effects of spin on the Kozai mechanism. We simulate merging binary black holes perturbed by a distant third mass. We calculate the gravitational waveforms produced by hierarchal triplet systems. Our methods are discussed in Chapter 2 and our results are presented in Chapter 3.

2 Methods

In this chapter we discuss our methods. A description of the post-Newtonian approximation and the Hamiltonian used in this work is given. Initial conditions used in our simulations are provided. Numerical methods used to solve the post-Newtonian equations are discussed. We describe the methods used to test our numeric solutions for the post-Newtonian equations at each order. Our method for calculating gravitational wave signals is discussed.

2.1 Post-Newtonian Approximation

The full Einstein equations of general relativity are nonlinear, partial differential equations. Solving these equations directly for three-body systems would be computationally expensive. Therefore, we use an alternative method, the post-Newtonian approximation. The post-Newtonian approximation consists of adding perturbations to the Newtonian Hamiltonian to correct for deviations from Einstein's equations. This expansion is valid when the relative velocity of the objects is not a significant fraction of the speed of light $(v/c)^2 \ll 1$ and the Newtonian potential is not too large $GM/rc^2 \ll 1$. The Hamiltonian used in this work is

$$H = H_N + H_{PN1} + H_{PN2} + H_{PN2.5} + H_{SO}^{LO} + H_{SaSb}^{LO} + H_S^{LO}. \quad (2.1)$$

The first term H_N is the Newtonian Hamiltonian. All subsequent terms are corrections to Newtonian gravity from general relativity. The first and second order corrections (H_{PN1} and H_{PN2}) alter the energy and trajectories of each mass, but still describe conservative systems. The two and a half order correction $H_{PN2.5}$ includes energy dissipation due to gravitational waves. The last three terms in Eq. (2.1) account for spin coupling effects to leading order. Specifically,

H_{SO}^{LO} accounts for coupling between the spin and orbital angular momentum of the objects, $H_{S_a S_b}^{LO}$ describes coupling between the spin angular momenta of different objects, and $H_{s^2}^{LO}$ accounts for effects caused by the deformation of objects due to their rotation. These corrections are given in Appendix A. One goal of this project is to study the dynamics of hierarchal three-body systems at varying orders in the post-Newtonian Hamiltonian.

With the Hamiltonian given by Eq. (2.1), the equations of motion are obtained through Hamilton's equation with an addition to account for spin effects,

$$\begin{aligned}
\frac{d\mathbf{X}_a}{dt} &= \frac{\partial H}{\partial \mathbf{P}_a} \\
\frac{d\mathbf{P}_a}{dt} &= -\frac{\partial H}{\partial \mathbf{P}_a} \\
\frac{d\mathbf{S}_a}{dt} &= \frac{\partial H}{\partial \mathbf{S}_a} \times \mathbf{S}_a
\end{aligned} \tag{2.2}$$

where \mathbf{X}_a , \mathbf{P}_a , and \mathbf{S}_a denote the position, conjugate momentum, and spin angular momentum of mass a respectively. The derivatives of the Hamiltonian in these equations are taken symbolically in Mathematica and the equations of motion are exported as optimized Fortran code. This code is included as a subroutine to solve the equations numerically in Julia.

2.2 Initial Conditions and Parameters

In this work, we study the Kozai mechanism and other nonlinear effects in hierarchal three-body systems. Hierarchal three-body systems can be treated as two effective one-body problems corresponding to the inner and outer binaries. It is convenient to specify these orbits in terms of Keplerian Orbital elements. The orbits for inner and outer binaries are specified in terms of their minor radius a , eccentricity e , inclination i , longitude of the ascending node Ω ,

argument of periastron ω , and mean anomaly M . A description of these orbital elements as well as relations for converting between orbital elements and Cartesian coordinates is given in Appendix B.

For all our simulations, the inclination of the outer binary is $i_{out} = 0^\circ$. The longitude of the ascending node Ω is initially 0 for both inner and outer orbits. The mean anomaly M is set as 0° and 20° for inner and outer orbits respectively. The models we simulate are given in Table 2.1. The PNN model consists of three equal mass pulsars. In the PNIB the inner binary consists of equal mass pulsars and the tertiary object is an intermediate mass black hole. In the PBIB model the inner binary consists of a neutron star and solar mass black hole, while the tertiary object is an intermediate mass black hole. In the PNB1 model the inner binary consists of a solar mass black hole and a pulsar, while another pulsar is the tertiary mass. The PNB2 model consists of the same objects as the PNB1 model, but the solar mass black hole is the outer mass. All masses in Table 2.1 are expressed in solar masses M_\odot . The initial conditions are specified in terms of Keplerian elements and converted to Cartesian coordinates for the simulations.

Model	$m_1(M_\odot)$	$m_2(M_\odot)$	$m_3(M_\odot)$	a_{in} (km)	a_{out}/a_{in}	e_{in}	e_{out}	i_{rel}°
PNN	1.4	1.4	1.4	1000	20	0.01	0.0	60
PNIB	1.4	1.4	10^3	5000	50	0.01	0.0	60
PBIB	30	1.4	10^3	10^6	50	0.01	0.0	60
PNB1	10	1.4	1.4	10^4	5	0.95	0.6	90
PNB2	1.4	1.4	10	10^5	20	0.6	0.95	90

Table 2.1 Tabulates masses in solar mass, inner minor radius a_{in} , ratio of outer to inner radius a_{out}/a_{in} , eccentricity of the inner binary e_{in} , eccentricity of the outer binary e_{out} , and relative inclination i_{rel} (in degrees) for each simulation model.

2.3 Numerical Methods and Tests

2.3.1 Integration Method and Units

The equations of motion in Eq. (2.2) are solved numerically using Julia. This program calls a Fortran subroutine for evaluating time derivatives at each step. We use Julia's Vern9 integrator with a relative and absolute error of 10^{-12} . Vern9 is a ninth order Runge-Kutta method utilizing adaptive step sizes. Adaptive step sizes are important in our simulations where systems may transition between quasi periodic motion and chaos. Simulations are run on Brigham Young University's Mary-lou supercomputer.

We use geometric units for our simulations, where $G = 1$ and $c = 1$. In these units the magnitude of the spin angular momentum of each object can be expressed in terms of its mass $\|\mathbf{S}_a\| = \chi_a m_a^2$, where $\chi_a \in (0,1)$. The unitless parameter χ_a is defined such that $\chi_a = 1$ denotes the object is maximally spinning. After performing simulations in geometric units the results are converted to SI units by multiplying the positions and time intervals by the scaling factors $R = GM / c^2$ and $T = GM / c^3$ where M denotes a mass scaling factor. We set this to one solar mass M_\odot . In this paper, after the mass values have been specified, all spin magnitudes are expressed in terms of χ_a .

2.3.2 Testing First and Second Order Post-Newtonian Equations

The Hamiltonian given in Appendix A is very complicated. Thus, we needed to test that the equations of motion in the code were inputted correctly and solved accurately at each order. At first and second post-Newtonian order, initial conditions for a binary system can be derived

that lead to circular orbits. We integrate the equations with these initial conditions and observe a constant separation distance. The process used to derive circular initial conditions for first and second post-Newtonian order is as follows. Given an initial radius R_0 we set $\phi_0 = 0$ and $\theta_0 = 0$, where $R_0, \phi_0 = 0, \theta_0 = 0$ are the spherical coordinates of the binary in the one-body frame. We then require the radial component of the conjugate momentum vanish $p_r(0) = 0$. Finally, we require \dot{p}_r and $\dot{\theta}$ initially vanish. By Hamilton's equations

$$\begin{aligned} (\dot{p}_r)_0 &= -\left(\frac{\partial H}{\partial r}\right)_0 = 0 \\ (\dot{\theta})_0 &= -\left(\frac{\partial H}{\partial p_\theta}\right)_0 = 0. \end{aligned} \tag{2.3}$$

These equations are solved numerically to obtain initial values for p_θ and p_ϕ . The equations of motion Eq. (2.2) were integrated with these circular initial conditions. Both masses were one solar mass and the initial separation was 500 km. The simulation was run for 10,000 orbits. The maximum relative error in the separation distance was less than 10^{-9} for both first and second order simulations. The three-body code was used for these simulations with the third body sufficiently far away that it didn't affect the solution.

2.3.3 Testing 2.5 Order and Spin Coupling Post-Newtonian Equations

For two and a half post-Newtonian order there are no initial conditions that lead to stable circular orbits. This is because gravitational waves will slowly radiate away the energy of a binary system causing the objects to in-spiral until they merge. In the case of a binary with the circular initial conditions described in Sec. 2.3.2, the separation distance as a function of time predicted by theory is given by

$$R(t) = R_0 \left(\frac{\tau - t}{\tau - t_0} \right), \quad (2.4)$$

where R_0 is the separation distance at some initial time t_0 . The characteristic time τ is given by

$$\tau = \frac{5}{256} \frac{c^5 R_0^4}{G^3 (m_1 + m_2)^2 \mu} \quad (2.5)$$

where $\mu = m_1 m_2 / (m_1 + m_2)$ is the reduced mass. Figure 2.1 shows close agreement between a simulated in-spiral and the prediction made by theory. The coordinate time is not Lorentz invariant and was scaled by a constant to make the fit.

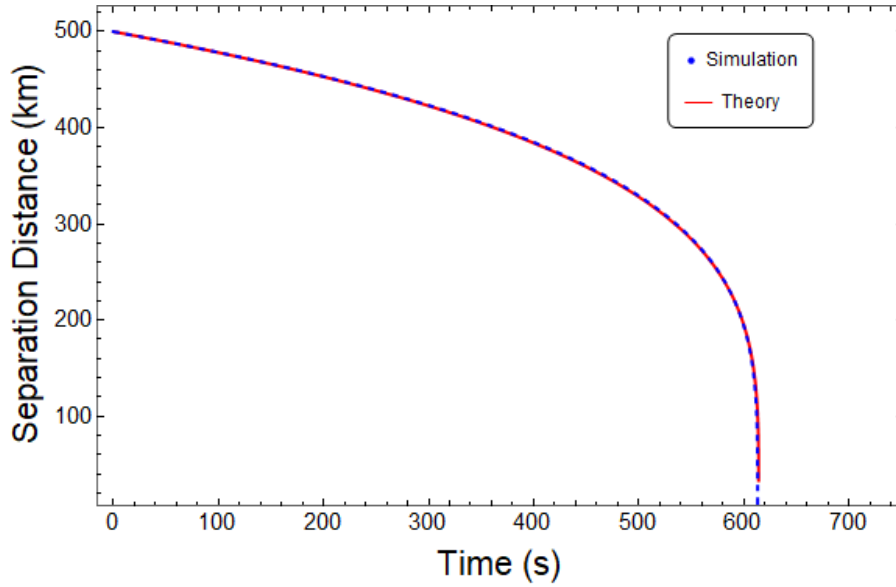


Fig. 2.1 Separation distance between two bodies satisfying the initially circular conditions described in Sec. 2.3.2. Each mass was one solar mass with an initial separation distance of 500 km. Simulation results are shown in blue and theoretical prediction Eq. (2.4) is shown in red.

There are no analytic solutions to the post-Newtonian equations to compare with when spin coupling terms are included. However previous work has been done performing simulations with post-Newtonian equations including spin coupling [11]. The post-Newtonian equations

were solved including terms through second order and leading order spin coupling terms for two-body systems. Our integrator replicated the trajectories in their paper. An example is given in Fig. 2.2.

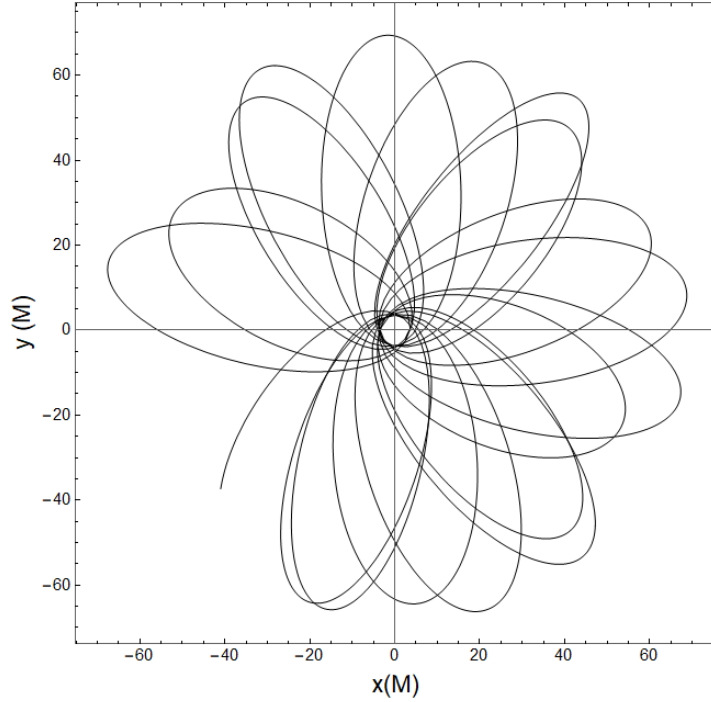


Fig. 2.2 Two-body simulation with spin coupling replicating the second figure in [11]. Each mass was $10 M_{\odot}$ with an initial eccentricity of $e = 0.9$ and pericenter radius of $r_p = 3.7$. Distances are measured in terms of the total mass in geometric units. Each body was maximally spinning with spins $S_1 = (1/\sqrt{2}, 0, 1/\sqrt{2})m_1^2$ and $S_2 = (1/2, 0, \sqrt{3}/2)m_2^2$. This plot is the trajectory in the one-body frame.

2.4 Gravitational Waves

2.4.1 Quadrupole Theory of Gravitational Waves

In addition to calculating the trajectories of masses in three-body systems, we calculate the gravitational waves produced by these systems to quadrupole order [12]. In this section we

present our methods for calculating these waveforms. All mathematical expressions in this section are given in geometric units, where $G = 1$ and $c = 1$. We calculate the gravitational waves propagating in a direction denoted by $\hat{\mathbf{n}} = \frac{\mathbf{x}}{r}$ where \mathbf{x} is the observation point and $r = \|\mathbf{x}\|$. We calculate the projector $\Lambda_{ij,kl}$ defined as

$$\Lambda_{ij,kl} = P_{ik}P_{jl} - \frac{1}{2}P_{ij}P_{kl} \quad (2.6)$$

where $P_{ij} = \delta_{ij} - n_i n_j$ and n_i denotes the i_{th} spatial component of $\hat{\mathbf{n}}$. The quadrupole moment Q_{ij} for a system of point masses is defined by

$$Q_{ij} = \sum_{\nu} m_{\nu} \left(x_{i,\nu} x_{j,\nu} - \frac{1}{3} \delta_{ij} \mathbf{x}_{\nu}^2 \right). \quad (2.7)$$

The indices i and j denote spatial components while the index ν is used to sum over all masses.

The quadrupole formula for the gravitational wave signal is

$$h_{ij}^{TT} = (t, \mathbf{x}) = \frac{2}{r} \Lambda_{ij,kl}(\hat{\mathbf{n}}) \frac{d^2 Q_{kl}}{dt^2}(t - r). \quad (2.8)$$

Summation over the k and l indices is implied by the Einstein summation convention. The tensor given by Eq.(2.8) has nine components, but only two degrees of freedom. These can be conveniently extracted by introducing two unit vectors $\hat{\mathbf{p}}$ and $\hat{\mathbf{q}}$ that are orthogonal to the propagation direction $\hat{\mathbf{n}}$, and to each other. The tensor h_{ij}^{TT} is decomposed into two independent “cross” and “plus” polarizations

$$h_{ij}^{TT} = h_{+}(p_i p_j - q_i q_j) + h_{\times}(p_i q_j + q_i p_j). \quad (2.9)$$

Equation (2.8) does not include spin effects in the gravitational waves.

2.4.2 Numeric Implementation and Testing

We calculate the gravitational wave signal given by Eq.(2.8) numerically for three-body systems. We solve the post-Newtonian equations of motion Eq.(2.2) in Julia and save the position, velocity, and acceleration at each time step. We substitute these the quantities into the analytic expression of the quadrupole moment $\frac{\partial^2 Q_{kl}}{\partial t^2}$ to calculate the tensor h_{ij}^{TT} . This tensor is calculated in cartesian coordinates and then converted to the basis $\hat{\mathbf{p}}$, $\hat{\mathbf{q}}$, and $\hat{\mathbf{n}}$ to extract the polarizations h_+ and h_\times . The waveforms fall off with the distance to the observer r . For our calculations we set this to unity in simulation units ($G = 1, c = 1, M_\odot = 1$).

The polarizations h_+ and h_\times can be calculated exactly for the case of a binary in a circular orbit moving under Newtonian gravity [12]. In this case the gravitational waves emitted parallel to the orbital angular momentum are

$$\begin{aligned} h_+(t) &= \frac{4\mu}{r} (\Omega R)^2 \cos(2\Omega(t-r)) \\ h_\times(t) &= \frac{4\mu}{r} (\Omega R)^2 \sin(2\Omega(t-r)), \end{aligned} \tag{2.10}$$

where $\mu = m_1 m_2 / (m_1 + m_2)$ is the reduced mass, $\Omega = \sqrt{\frac{m_1 + m_2}{R^3}}$ is the orbital frequency and R is the separation distance of the binary. Figure 2.3 shows close agreement between a numerically calculated waveform and Eq.(2.10). The Newtonian Hamiltonian was used for the simulation.

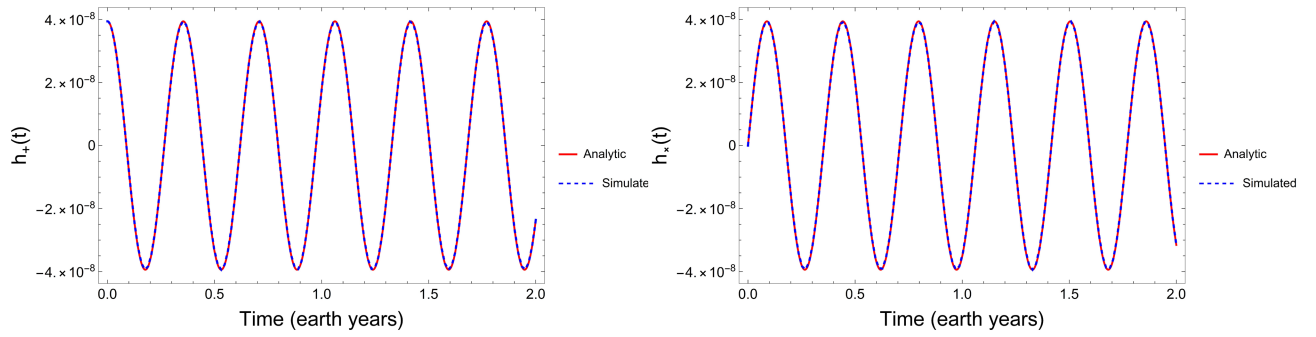


Fig. 2.2 The h_+ and h_x polarizations of gravitation waves emitted from a binary in a circular orbit. The initial separation distance was $R = 1$ (au) and each object was one solar mass. Each plot shows close agreement between numeric simulation in blue and Eq.(2.10) in red. The Newtonian Hamiltonian was used for the numerical simulation.

3 Results and Conclusions

In this chapter we discuss our results from simulating the post-Newtonian three-body problem. We show representative examples of our simulations from the models tabulated in Table 2.1. We focus on simulations of compact systems, where relativistic effects play the largest role. Simulation results show that spin coupling effects can alter Kozai oscillations. The spin angular momentum of each object is constant in magnitude, but changes orientation. We also discuss how the dynamics of the Kozai mechanism change with post-Newtonian Order. We characterize how the Kozai mechanism varies with separation distance. We give examples in which spin effects alter the merge time of black holes and neutron stars. We show simulation examples of gravitational waves radiated from a hierarchal triplet system. Applications of this research will be discussed.

3.1 Spin Angular Momentum Coupling

3.1.1 Spin Effects on Kozai Mechanism

We solved the post-Newtonian equations with spin coupling terms included to leading order as described in Sec. 2.4 of chapter 2. The spin coupling terms are higher order in v/c and spin effects can often be neglected². However, when analyzing compact, massive systems, spin

² The leading order spin-orbit coupling terms are of order $(v/c)^3$. The other spin terms in our Hamiltonian are of order $(v/c)^4$.

coupling can have a significant effect on long term orbital resonances such as the Kozai mechanism.

Simulation results from the PBIB, PNIB, and PNN models are shown in Fig. 3.1. The rows from the top down correspond to simulations of the PBIB, PNIB, and PNN models, respectively. The eccentricity of the inner binary averaged over an orbital period is shown. The left column contrasts Kozai oscillations for the case in which none of the objects were spinning and the case where both masses of the inner binary were maximally spinning ($\chi_1 = \chi_2 = 1$) with their spin angular momentum parallel and in the orbital plane. The right column depicts simulations with the same initial conditions and parameters, but the spin angular momenta of the masses in the inner binary are oriented perpendicular to the orbital plane.

Figure 3.1 shows several effects spin coupling can have on the Kozai mechanism. In the PBIB model the spin effects cause an increase in the frequency of Kozai oscillations while the amplitude is nearly constant. In both the PNIB and PNN models, spin effects introduce new irregularities in the frequency and amplitude of Kozai oscillations. The PNN model doesn't have steady KL oscillations, even in the absence of spin. This is because the inner binary is sufficiently compact that energy dissipation due to gravitational waves and other relativistic effects plays a more dominant role.

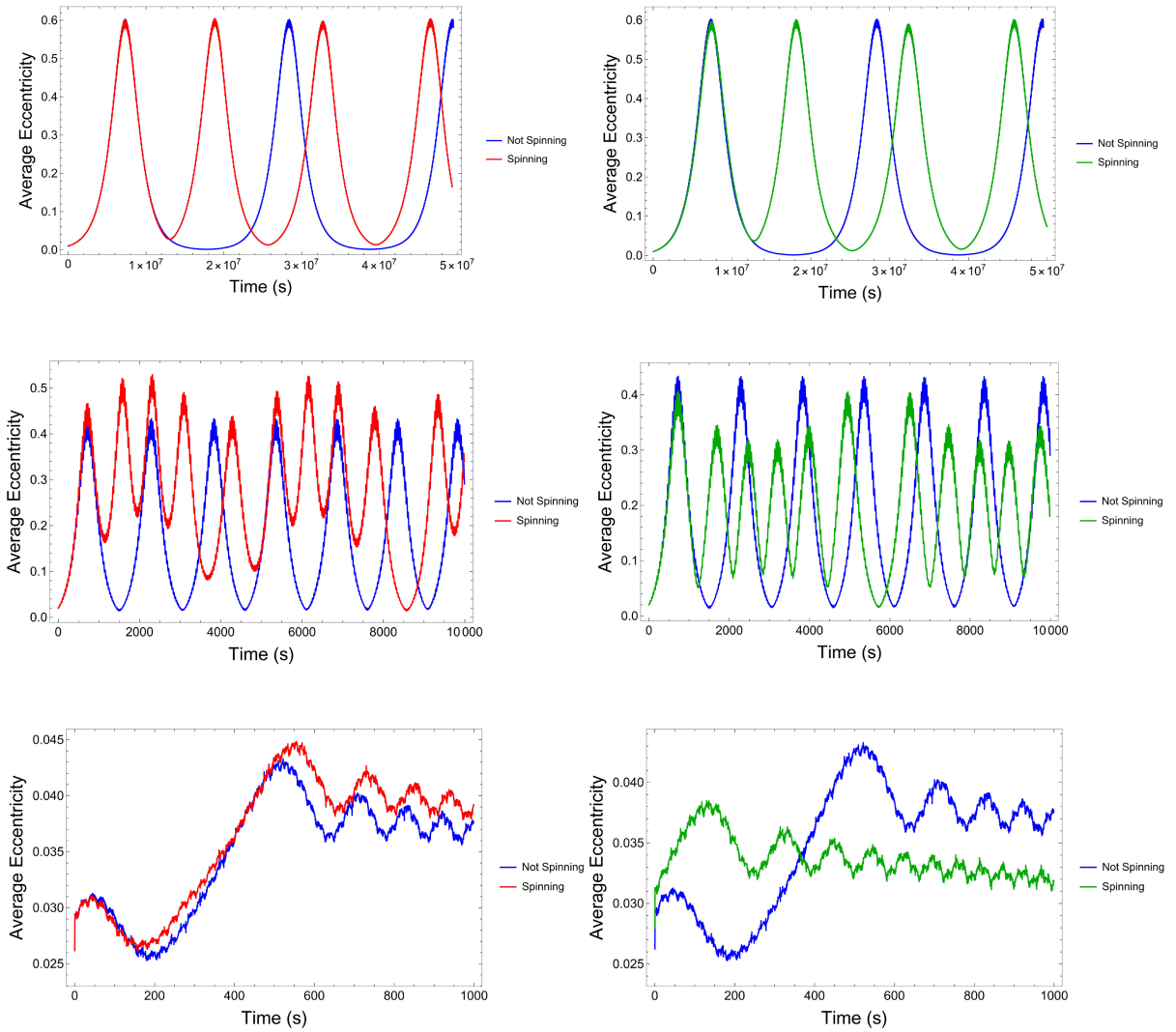


Fig. 3.1 The eccentricity of the inner binary averaged over an orbital period. The rows from the top down correspond to simulations of the PBIB, PNIB, and PNN models respectively. The left column contrast Kozai oscillations for the case in which none of the objects were spinning and the case where both masses of the inner binary were maximally spinning with their spin angular momentum parallel, lying in the orbital plane. The right column shows simulations with the same initial conditions and parameters, but the spin angular momenta of the masses in the inner binary are oriented perpendicular to the orbital plane.

3.1.2 Evolution of Spin Angular Momenta

The magnitude of the spin angular momentum of each mass is a conserved quantity in the post-Newtonian Hamiltonian, with spin terms included to leading order [11]. However, our simulations show that the orientation of the object's spin angular momenta is not constant. Simulation results showing the time evolution of the spin angular momentum for PBIB, PNIB, and PNN models are shown in Fig.3.2. The rows correspond to the PNN, PNIB, and PBIB models respectively. In each simulation all three masses were initially maximally spinning ($\chi_1 = \chi_2 = \chi_3 = 1$) with each mass's spin vector initially oriented parallel to its orbital angular momentum. The spin angular momenta of each mass are represented as tracing out trajectories on the surface of a sphere with radius $\chi = 1$. During the integration time shown for each simulation, the inner binary undergoes many orbits. The inner binary undergoes 3,300 orbits in the PNN simulation, 2,700 orbits in the PNIB simulation, and 32,500 orbits in the PBIB simulation. In each case the spin angular momentum of each object evolves on a timescale longer than an orbital period. In each simulation, the trajectories traced out by the spin angular momenta of the inner masses are nearly identical. This is even true for the PBIB model where the inner binary is not composed of equal mass objects.

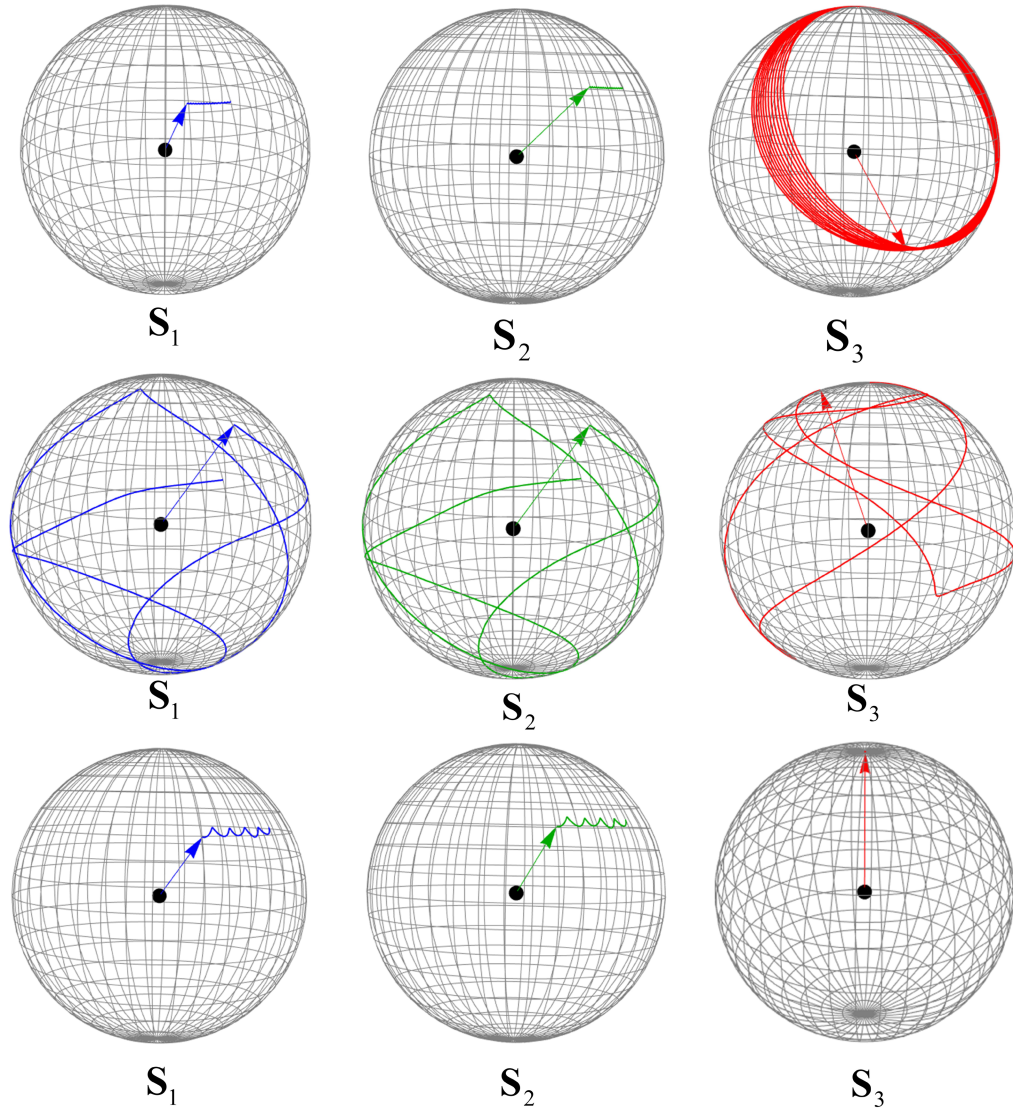


Fig. 3.2 Evolution of the spin angular momentum for each mass in the PNN, PNIB and PBIB models. In all simulations each mass was maximally spinning with its spin angular momentum parallel to its orbital angular momentum. The spin angular momenta of each mass are constant in magnitude but vary in orientation. The spin angular momenta are represented as tracing out trajectories on the surface of a sphere with radius $\chi = 1$. In each model the spin angular momentum of each mass evolves on a timescale longer than orbital period.

3.2 Comparing Post-Newtonian Orders

Our simulations show Kozai oscillations occur through two and a half order in the post-Newtonian expansion in all models shown in Table 2.1. The amplitude and frequency of these oscillations vary with post-Newtonian order. Simulation results from the PNN, PNIB, and PBIB models at varying post-Newtonian order are shown in Fig. 3.3. The first and second order terms describe conservative systems. We find the Kozai mechanism can exhibit steady state oscillations at first and second order. However, at two and a half order, emission of gravitational waves causes Kozai oscillations to vary in frequency and amplitude over time. Eventually gravitational waves will drive the objects of the inner binary sufficiently close together that relativistic effects dominate over the Kozai mechanism.

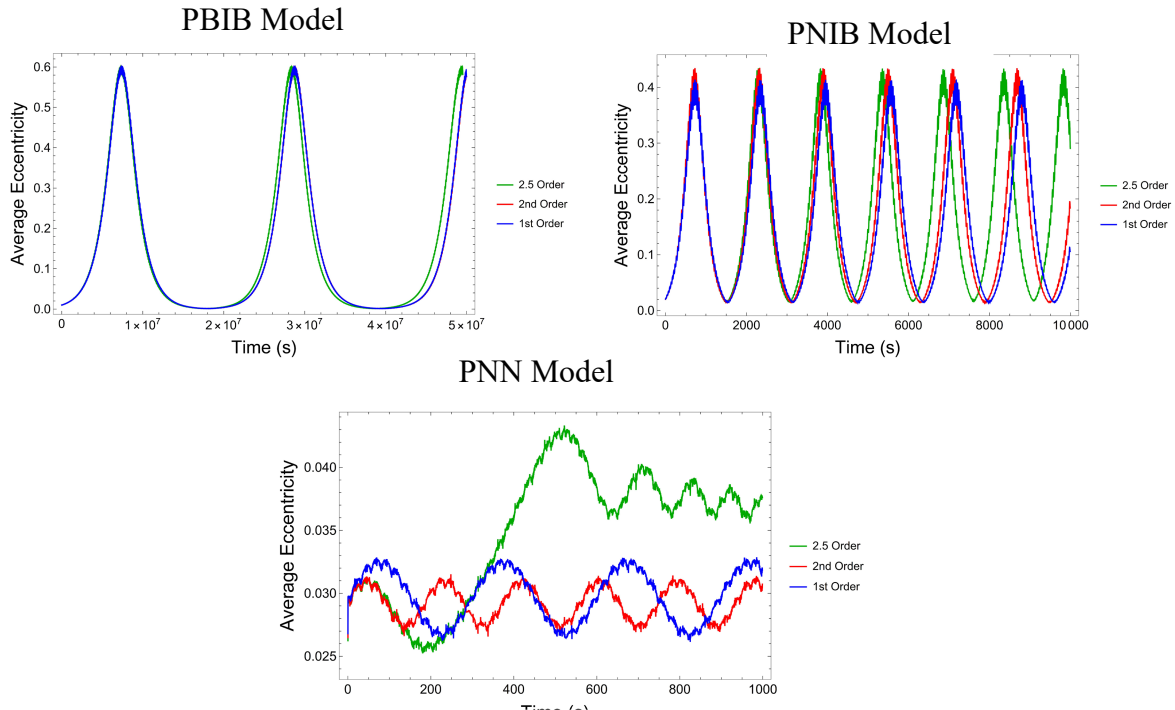


Fig. 3.3 Eccentricity of the inner binary averaged over each orbital period at varying post-Newtonian orders in the PBIB, PNIB and PNN models.

3.3 Radial Dependence

Our simulations show that Kozai oscillations decrease in amplitude as the objects get closer together and relativistic effects dominate. We also find the orbital period of Kozai oscillations increase with separation distance. The amplitude and period of the oscillations in the average eccentricity of the inner binary for the PNN model are shown in Fig. 3.4.

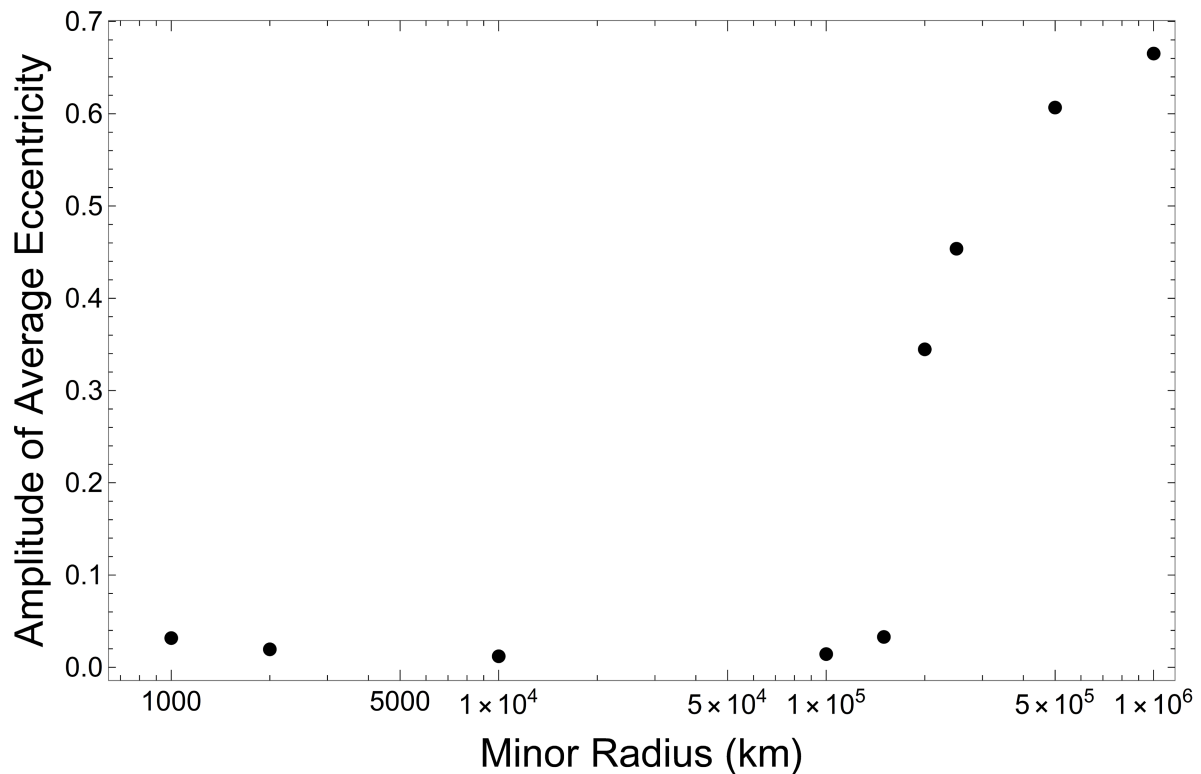


Fig. 3.4 (a) Amplitude of averaged eccentricity of the inner binary for PNN model at varying inner minor radius a_{in} . Results from solving the post-Newtonian equations at second order are plotted.

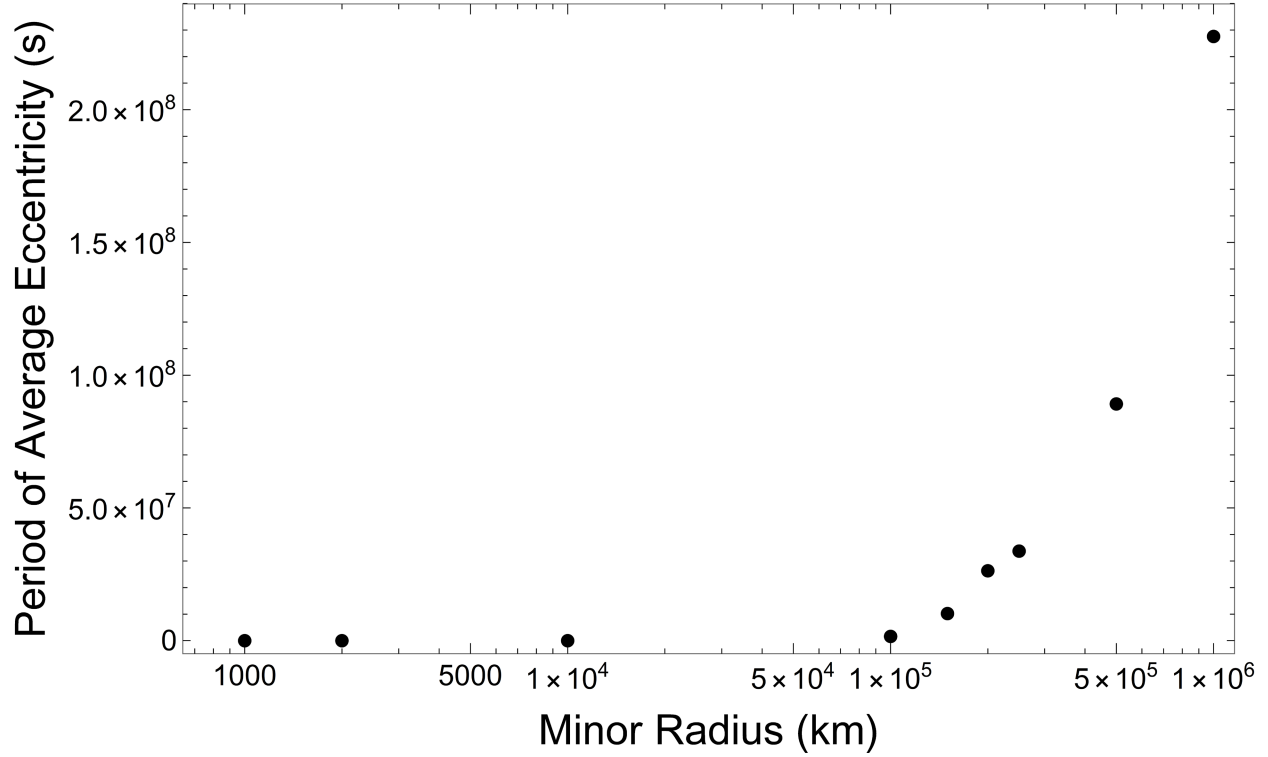


Fig. 3.4 (b) Period of Kozai oscillations for PNN model at varying inner minor radius a_m . Results from solving the post-Newtonian equations at second order are plotted.

3.4 Spin Effects on Merge Times

In this section we give examples of simulation results to show the potential for spin coupling effects to alter the time it takes black holes to merge within a hierarchal triplet system. The separation distance of the inner binary averaged over an orbital period for a system in the PNB2 model is given in Fig. 3.5. The blue curve shows a simulation result in which all three bodies are not spinning. The red curve shows results of a simulation in which only one mass of the inner binary was spinning with magnitude $\chi_2 = 1$, and initially oriented in the orbital plane. In the simulation with spin the inner binary merges at 73% the time of the simulation without spin.

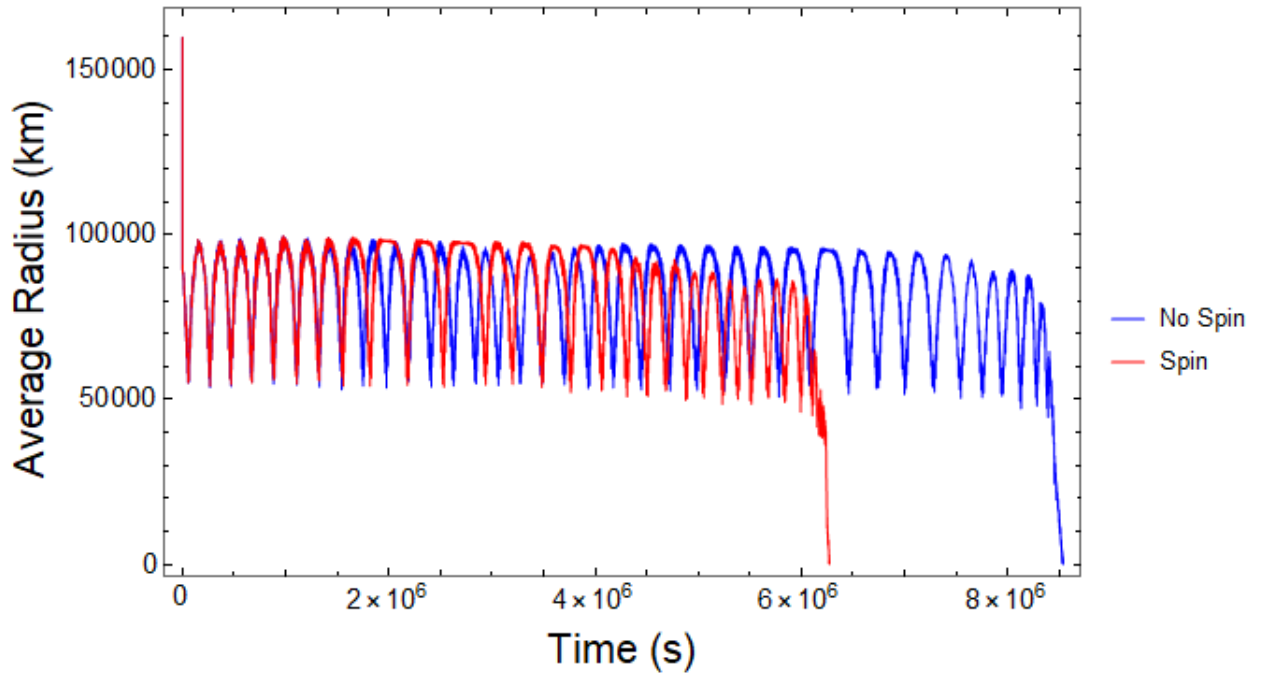


Fig. 3.5 The separation distance of the inner binary averaged over an orbital period for a system in the PNB2 model is given in Fig. 3.5. The blue curve shows a simulation result in which all three bodies were not spinning. The red curve shows results of a simulation in which only one mass of the inner binary was spinning with magnitude $\chi_2 = 1$ and initially oriented in the orbital plane. In the simulation with spin the inner binary merges at 73% the time of the simulation without spin.

The averaged separation distance of the inner binary for simulations in the PNB1 model is given in Fig. 3.6. The blue curve is the result of a simulation in which none of the objects were spinning. The red curve is the result of a simulation in which only the tertiary mass was spinning with magnitude $\chi_3 = 1$ initially oriented perpendicular to the orbital plane. In this case spin caused the objects to merge slower by a factor of 2.1.

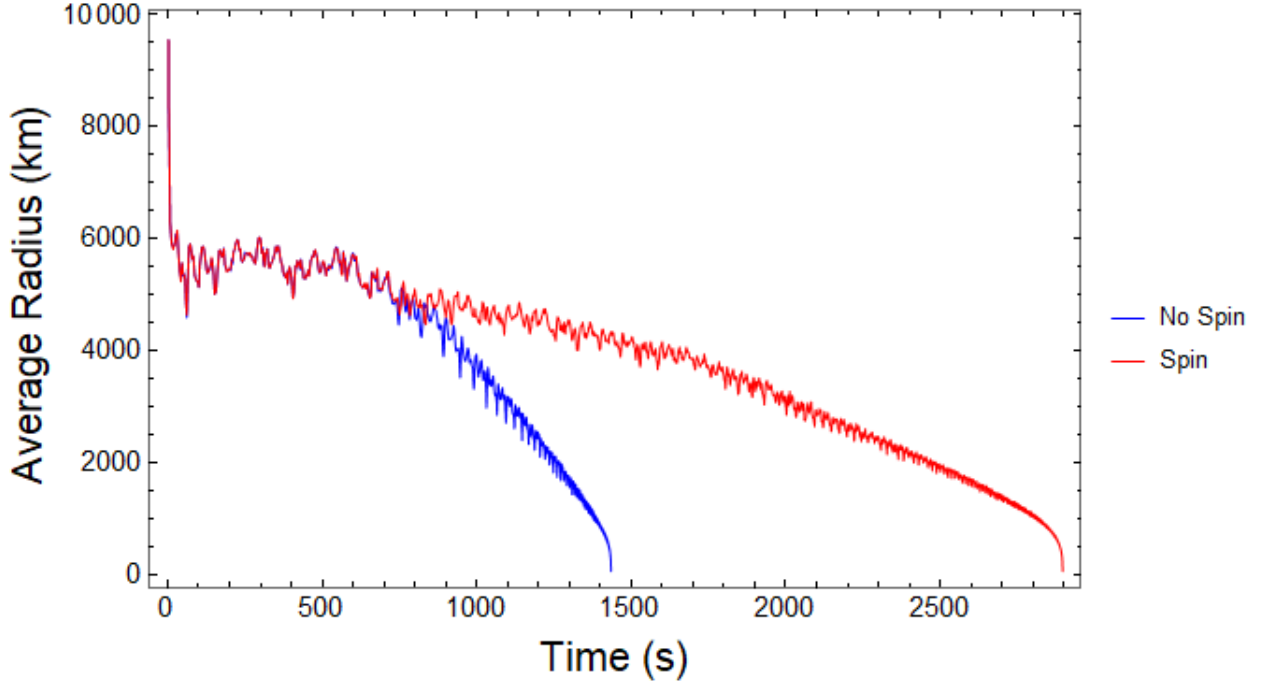


Fig. 3.6 The averaged separation distance of the inner binary for simulations in the PNB1 model. The blue curve is the result of a simulation in which none of the objects were spinning. The red curve is the result of a simulation in which only the tertiary mass was spinning with magnitude initially oriented perpendicular to the orbital plane. In this case spin caused the objects to merge slower by a factor of 2.1.

3.5 Gravitational Wave Simulations

We computed gravitational wave forms at quadrupole order as discussed in Sec. 2.4.

These waveforms are represented in terms of two independent polarizations h_+ and h_\times . Here we give examples from simulating the PNN model. Figure 3.7 shows gravitational waves produced in the PNN model (Left) and a system with the same masses and initial conditions, but with the third body removed (Right). Figure 3.7 shows the components of gravitational waves propagating perpendicular to the orbital plane of the outer binary in the PNN model. Each simulation is plotted for 26 seconds, during which time the separation distance of the inner

binary in the PNN model decreases to 95% of its initial value and the separation distance in the two-body simulation decreases to 96% its initial value. In both simulations the gravitational waves oscillate at a frequency of about twice the orbital frequency. Interactions with the third body introduce oscillations at an additional, lower frequency in the PNN model that is not present in the two-body simulation.

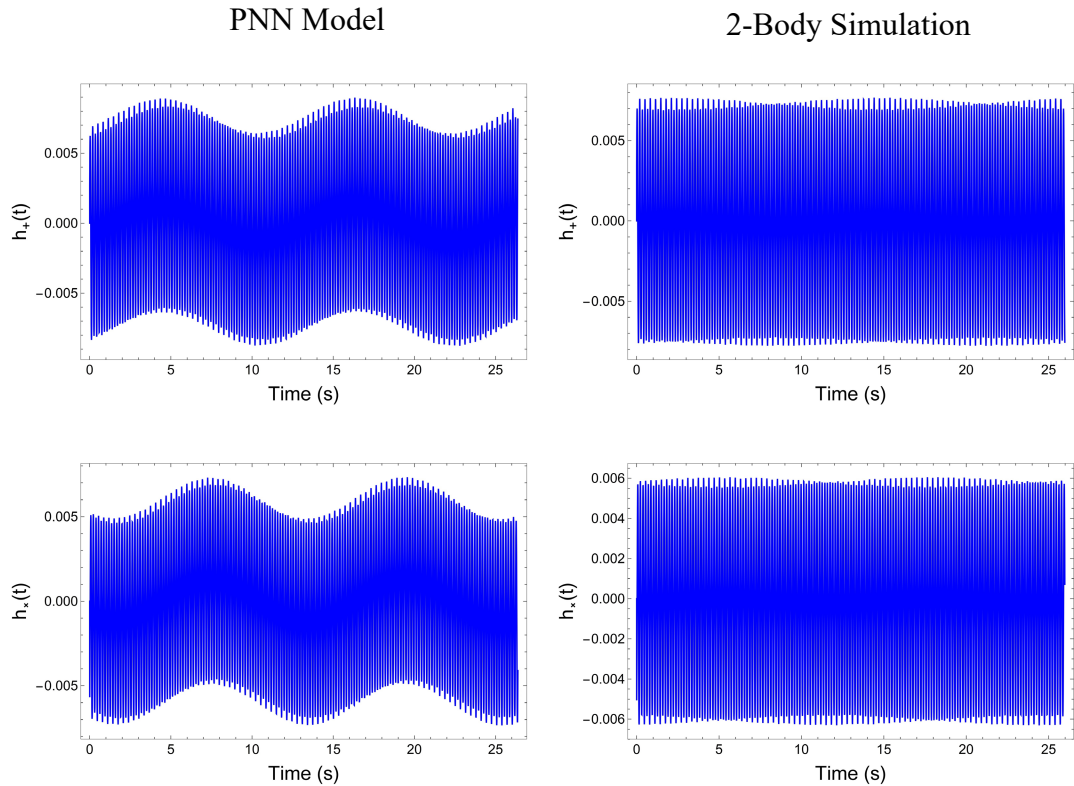


Fig. 3.7 Gravitational waves produced in the PNN model (Left) and a system with the same masses and initial conditions, but with the third body removed (Right). In both simulations the gravitational waves oscillate at a frequency of about twice the orbital frequency. Interactions with the third body introduce oscillations at an additional, lower frequency that is not present in the two-body simulation.

The gravitational waves that are detectable by LIGO result from the last few orbits before a binary composed of black holes or neutron stars merge. Figure 3.8 shows the gravitational waves leading up to the merger event for the same systems as in Fig. 3.7. We see that while three-body

interactions play a major role when the objects are about 5,000 km apart (Fig 3.7), they have little effect on the final signal shown in Fig. 3.8.

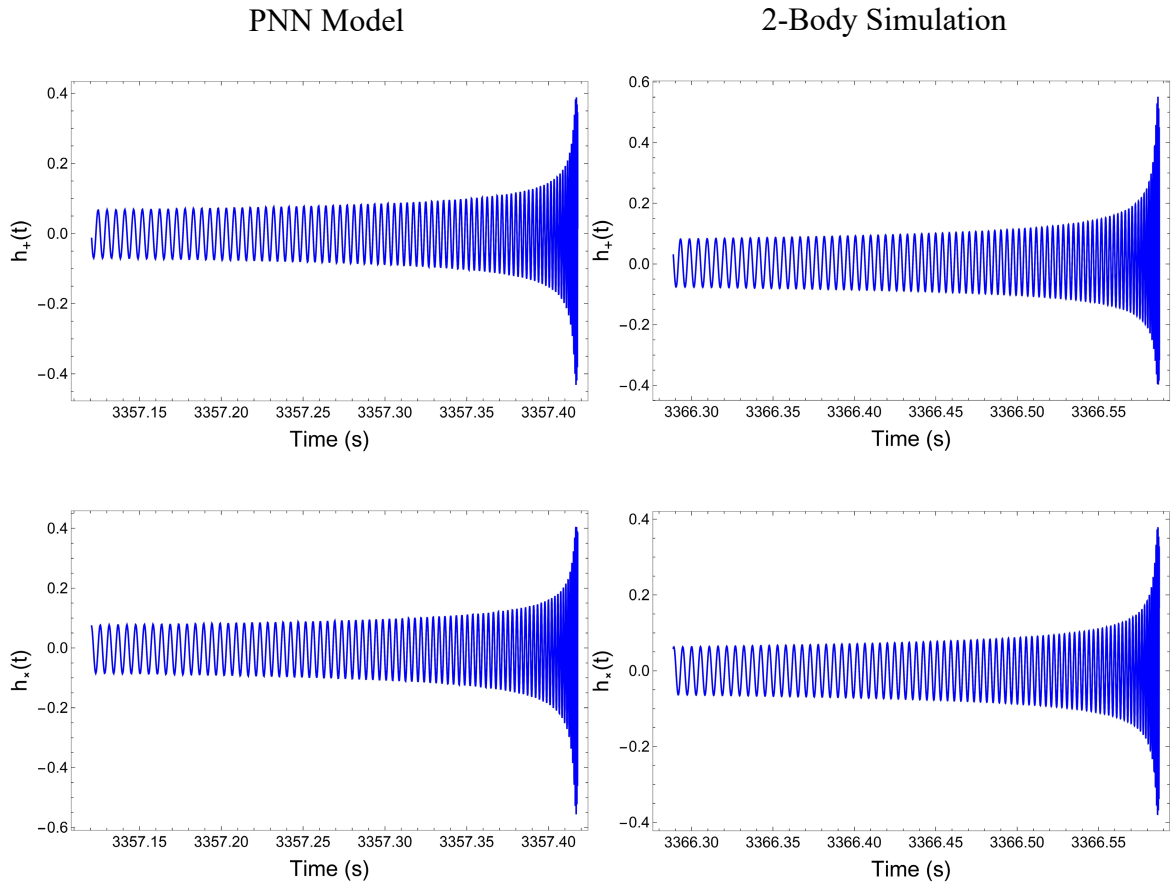


Fig. 3.8 Gravitational waves produced in the PNN model (Left) and a system with the same masses and initial conditions, but with the third body removed (Right). The final signal before the objects merge is shown.

3.6 Conclusion

In this work we used the post-Newtonian approximation of Einstein's equations of general relativity to study the Kozai mechanism. The Kozai mechanism is an orbital resonance occurring in hierarchal three-body systems characterized by long term oscillations between the eccentricity of the inner binary and relative inclination. We simulated this effect for systems composed of pulsars and black holes. We found that coupling between the spin angular momenta of the objects can alter Kozai oscillations. The spin angular momenta of the objects remain constant in magnitude but change orientation. Predictions of both the trajectories of the masses, and orientation of the spin angular momenta would be relevant when comparing observations of triplet pulsar systems with predictions from general relativity. Such a study would be a new test of general relativity.

We simulated the Kozai mechanism at different post-Newtonian orders. The inclusion of two and half order post-Newtonian terms causes variations from the steady state Kozai oscillations possible at lower orders. We also find that the amplitude and period of Kozai oscillations decrease with separation distance when the objects are sufficiently close that relativistic effects dominate. Additionally, we simulated black hole and neutron star mergers in hierarchal triplet systems. We found evidence for cases in which spin effects altered the merger time of the inner binary. Our code could be used to conduct further research on this topic. Simulations could investigate which parameters play an important role in spin effecting merge times. More runs may determine if spin can have a significant effect on merge times when the initial separation distances are large. We also calculated gravitational waves radiated from hierarchal triplet systems. We found the tertiary mass could induce oscillations at an additional,

lower frequency, but this effect was diminished when the inner binary was sufficiently close to merging. Future research could determine possible effects three-body interactions may have on the gravitational waves observed by LIGO.

Appendix A

Post Newtonian Hamiltonian

In this appendix we give the post-Newtonian Hamiltonian we used to derive the equations of motion for three-body systems. The Hamiltonian consists of the Newtonian Hamiltonian H_N with additional perturbations to correct for deviations from Einstein's equations. The Hamiltonian used in this work is

$$H = H_N + H_{PN1} + H_{PN2} + H_{PN2.5} + H_{SO}^{LO} + H_{SaSb}^{LO} + H_{S^2}^{LO}. \quad (\text{A.1})$$

The equations of motion are then obtained through Hamilton's equations with an addition to account for spin effects,

$$\begin{aligned} \frac{d\mathbf{X}_a}{dt} &= \frac{\partial H}{\partial \mathbf{P}_a} \\ \frac{d\mathbf{P}_a}{dt} &= -\frac{\partial H}{\partial \mathbf{P}_a} \\ \frac{d\mathbf{S}_a}{dt} &= \frac{\partial H}{\partial \mathbf{S}_a} \times \mathbf{S}_a. \end{aligned} \quad (\text{A.2})$$

The Hamiltonian is expressed in units where $G = 1$ and $c = 1$. The Newtonian Hamiltonian is

$$H_N = \frac{1}{2} \sum_a \frac{p_a^2}{m_a} - \frac{1}{2} \sum_{a,b \neq a} \frac{m_a m_b}{r_{ab}}. \quad (\text{A.3})$$

Where p_a, m_a are the linear momentum and mass for object a and r_{ab} is the distance between m_a and m_b . The 1st order correction is

$$H_{PN1} = -\frac{1}{8} \sum_a m_a \left(\frac{p_a^2}{m_a^2} \right)^2 - \frac{1}{4} \sum_{a,b \neq a} \frac{m_a m_b}{r_{ab}} \left\{ 6 \frac{p_a^2}{m_a^2} - 7 \frac{\mathbf{p}_a \cdot \mathbf{p}_b}{m_a m_b} - \frac{(\mathbf{n}_{ab} \cdot \mathbf{p}_a)(\mathbf{n}_{ab} \cdot \mathbf{p}_b)}{m_a m_b} \right\} + \frac{1}{2} \sum_{a,b \neq a, c \neq a} \frac{m_a m_b m_c}{r_{ab} r_{ac}}, \quad (\text{A.4})$$

where \mathbf{n}_{ab} is the unit vector pointing from m_a to m_b . The second order correction is

$$H_{PN2} = \frac{1}{16} \sum_a m_a \left(\frac{p_a^2}{m_a^2} \right)^3 + \frac{1}{16} \sum_{a,b \neq a} \frac{m_a m_b}{r_{ab}} \left\{ 10 \left(\frac{p_a^2}{m_a^2} \right)^2 - 11 \frac{p_a^2 p_b^2}{m_a^2 m_b^2} - 2 \frac{(\mathbf{p}_a \cdot \mathbf{p}_a)^2}{m_a^2 m_b^2} + 10 \frac{p_a^2 (\mathbf{n}_{ab} \cdot \mathbf{p}_b)^2}{m_a^2 m_b^2} - 12 \frac{(\mathbf{p}_a \cdot \mathbf{p}_b)(\mathbf{n}_{ab} \cdot \mathbf{p}_a)(\mathbf{n}_{ab} \cdot \mathbf{p}_b)}{m_a^2 m_b^2} - 3 \frac{(\mathbf{n}_{ab} \cdot \mathbf{p}_a)^2 (\mathbf{n}_{ab} \cdot \mathbf{p}_b)^2}{m_a^2 m_b^2} \right\} + \frac{1}{8} \sum_{a,b \neq a, c \neq a} \frac{m_a m_b m_c}{r_{ab} r_{ac}} \left\{ 18 \frac{p_a^2}{m_a^2} + 14 \frac{p_b^2}{m_b^2} - 2 \frac{(\mathbf{n}_{ab} \cdot \mathbf{p}_b)^2}{m_b^2} - 50 \frac{\mathbf{p}_a \cdot \mathbf{p}_b}{m_a m_b} + 17 \frac{\mathbf{p}_b \cdot \mathbf{p}_c}{m_b m_c} - 14 \frac{(\mathbf{n}_{ab} \cdot \mathbf{p}_a)(\mathbf{n}_{ab} \cdot \mathbf{p}_b)}{m_a m_b} + 14 \frac{(\mathbf{n}_{ab} \cdot \mathbf{p}_b)(\mathbf{n}_{ab} \cdot \mathbf{p}_c)}{m_b m_c} + \mathbf{n}_{ab} \cdot \mathbf{n}_{ac} \frac{(\mathbf{n}_{ab} \cdot \mathbf{p}_b)(\mathbf{n}_{ac} \cdot \mathbf{p}_c)}{m_b m_c} \right\} + \frac{1}{8} \sum_{a,b \neq a, c \neq a} \frac{m_a m_b m_c}{r_{ab}^2} \left\{ 2 \frac{(\mathbf{n}_{ab} \cdot \mathbf{p}_a)(\mathbf{n}_{ac} \cdot \mathbf{p}_c)}{m_a m_c} + 2 \frac{(\mathbf{n}_{ab} \cdot \mathbf{p}_b)(\mathbf{n}_{ac} \cdot \mathbf{p}_c)}{m_a m_c} + 5 \mathbf{n}_{ab} \cdot \mathbf{n}_{ac} \frac{p_c^2}{m_c^2} - \mathbf{n}_{ab} \cdot \mathbf{n}_{ac} \frac{(\mathbf{n}_{ac} \cdot \mathbf{p}_c)^2}{m_c^2} - 14 \frac{(\mathbf{n}_{ab} \cdot \mathbf{p}_c)(\mathbf{n}_{ac} \cdot \mathbf{p}_c)}{m_c^2} \right\} + \frac{1}{4} \sum_{a,b \neq a} \frac{m_a^2 m_b}{r_{ab}^2} \left\{ \frac{p_a^2}{m_a^2} + \frac{p_b^2}{m_b^2} - 2 \frac{\mathbf{p}_a \cdot \mathbf{p}_b}{m_a m_b} \right\} + \frac{1}{2} \sum_{a,b \neq a, c \neq a, b} \frac{m_a m_b m_c}{(r_{ab} + r_{bc} + r_{ca})^2} (n_{ab}^i + n_{ac}^i)(n_{ab}^j + n_{cb}^j) \left\{ 8 \frac{p_{ai} p_{cj}}{m_a m_c} - 16 \frac{p_{aj} p_{ci}}{m_a m_c} + 3 \frac{p_{ai} p_{bj}}{m_a m_b} + 4 \frac{p_{ci} p_{cj}}{m_c^2} + \frac{p_{ai} p_{aj}}{m_a^2} \right\} + \frac{1}{2} \sum_{a,b \neq a, c \neq a, b} \frac{m_a m_b m_c}{(r_{ab} + r_{bc} + r_{ca}) r_{ab}} \left\{ 8 \frac{\mathbf{p}_a \cdot \mathbf{p}_c - (\mathbf{n}_{ab} \cdot \mathbf{p}_a)(\mathbf{n}_{ab} \cdot \mathbf{p}_c)}{m_a m_c} - 3 \frac{\mathbf{p}_a \cdot \mathbf{p}_b - (\mathbf{n}_{ab} \cdot \mathbf{p}_a)(\mathbf{n}_{ab} \cdot \mathbf{p}_b)}{m_a m_b} - 4 \frac{p_c^2 - (\mathbf{n}_{ab} \cdot \mathbf{p}_c)^2}{m_c^2} - \frac{p_a^2 - (\mathbf{n}_{ab} \cdot \mathbf{p}_a)^2}{m_a^2} \right\} - \frac{1}{2} \sum_{a,b \neq a, c \neq b} \frac{m_a^2 m_b m_c}{r_{ab}^2 r_{bc}} - \frac{1}{4} \sum_{a,b \neq a, c \neq a} \frac{m_a m_b m_c^2}{r_{ab} r_{ac}^2} + \frac{1}{2} \sum_{a,b \neq a} \frac{m_a^3 m_b}{r_{ab}^3} - \frac{3}{4} \sum_{a,b \neq a, c \neq a} \frac{m_a^2 m_b m_c}{r_{ab}^2 r_{ac}} - \frac{3}{8} \sum_{a,b \neq a, c \neq a, b} \frac{m_a^2 m_b m_c}{r_{ab} r_{ac} r_{bc}} + \frac{3}{8} \sum_{a,b \neq a} \frac{m_a^2 m_b^2}{r_{ab}^3} - \frac{1}{64} \sum_{a,b \neq a, c \neq a, b} \frac{m_a^2 m_b m_c}{r_{ab}^3 r_{ac}^3 r_{bc}} \left\{ 18 r_{ab}^2 r_{ac}^2 - 60 r_{ab}^2 r_{bc}^2 - 24 r_{ab}^2 r_{ac} (r_{ab} + r_{bc}) + 60 r_{ab} r_{ac} r_{bc}^2 + 56 r_{ab}^3 r_{bc} - 72 r_{ab} r_{bc}^3 + 35 r_{bc}^4 + 6 r_{ab}^4 \right\} - \frac{1}{4} \sum_{a,b \neq a} \frac{m_a^2 m_b^2}{r_{ab}^3}. \quad (\text{A.5})$$

The post-Newtonian Hamiltonian at two and a half order accounts for effects due to gravitational waves. This correction is given by

$$H_{PN2.5} = \frac{1}{45} \dot{\chi}_{(4)ij}(\mathbf{x}_{a'}, \mathbf{p}_{a'}; t) \chi_{(4)ij}(\mathbf{x}_a, \mathbf{p}_a), \quad (\text{A.6})$$

The quantities $\dot{\chi}_{(4)ij}(\mathbf{x}_{a'}, \mathbf{p}_{a'}, t)$ and $\chi_{(4)ij}(\mathbf{x}_a, \mathbf{p}_a, t)$ are defined by

$$\chi_{(4)ij}(\mathbf{x}_a, \mathbf{p}_a) = \sum_a \frac{2}{m_a} ((\mathbf{p}_a \cdot \mathbf{p}_a) \delta_{ij} - 3p_{ai}p_{aj}) + \sum_{a,b \neq a} \frac{m_a m_b}{r_{ab}} (3n_{abi}n_{abj} - \delta_{ij}), \quad (\text{A.7})$$

$$\begin{aligned} \dot{\chi}_{(4)ij}(\mathbf{x}_{a'}, \mathbf{p}_{a'}) &= \sum_{a'} \frac{2}{m_{a'}} \left[2(\dot{\mathbf{p}}_{a'} \cdot \mathbf{p}_{a'}) \delta_{ij} - 3(\dot{p}_{a'i}p_{a'j} + p_{a'i}\dot{p}_{a'j}) \right] \\ &+ \sum_{a',b' \neq a'} \frac{m_{a'} m_{b'}}{r_{a'b'}^2} \left[3(\dot{r}_{a'b'i}n_{a'b'j} + n_{a'b'i}\dot{r}_{a'b'j}) + (\mathbf{n}_{a'b'} \cdot \dot{\mathbf{r}}_{a'b'}) (\delta_{ij} - 9n_{a'b'i}n_{a'b'j}) \right], \end{aligned}$$

These expressions depend on the derivatives of the position and momenta. These are approximated using the 1st order Hamiltonian H_{PN1}

$$(\dot{\mathbf{x}}_a)_1 = -\frac{p_a^2}{2m_a^3} \mathbf{p}_a - \frac{1}{2} \sum_{b \neq a} \frac{1}{r_{ab}} \left(6\frac{m_b}{m_a} \mathbf{p}_a - 7\mathbf{p}_b - (\mathbf{n}_{ab} \cdot \mathbf{p}_b) \mathbf{n}_{ab} \right) \quad (\text{A.8})$$

$$\begin{aligned} (\dot{\mathbf{p}}_a)_1 &= -\frac{1}{2} \sum_{b \neq a} \left[3\frac{m_b}{m_a} p_a^2 - 7(\mathbf{p}_a \cdot \mathbf{p}_b) - 3(\mathbf{n}_{ab} \cdot \mathbf{p}_a)(\mathbf{n}_{ab} \cdot \mathbf{p}_a) \right] \frac{\mathbf{n}_{ab}}{r_{ab}^2} \\ &+ \sum_{b \neq a, c \neq a} \frac{m_a m_b m_c}{r_{ab}^2 r_{ac}} \mathbf{n}_{ab} + \sum_{b \neq a, c \neq b} \frac{m_a m_b m_c}{r_{ab}^2 r_{bc}} \mathbf{n}_{ab} - \frac{1}{2} \sum_{a \neq b} \left[\frac{(\mathbf{n}_{ab} \cdot \mathbf{p}_b) \mathbf{p}_a + (\mathbf{n}_{ab} \cdot \mathbf{p}_a) \mathbf{p}_b}{r_{ab}^2} \right]. \end{aligned} \quad (\text{A.9})$$

The spin coupling corrections are

$$H_{SO}^{LO} = \sum_a \sum_{b \neq a} \frac{1}{r_{ab}^2} (\mathbf{S}_a \times \mathbf{n}_{ab}) \cdot \left(\frac{3m_b}{m_a} \mathbf{p}_a - 2\mathbf{p}_b \right), \quad (\text{A.11})$$

$$H_{S_a S_b}^{LO} = \sum_a \sum_{b \neq a} \frac{1}{2r_{ab}^3} [3(\mathbf{S}_a \cdot \mathbf{n}_{ab})(\mathbf{S}_b \cdot \mathbf{n}_{ab}) - (\mathbf{S}_a \cdot \mathbf{S}_b)], \quad (\text{A.12})$$

$$H_{S^2}^{LO} = \sum_a \sum_{b \neq a} \frac{m_b}{2m_a r_{ab}^3} [3(\mathbf{S}_a \cdot \mathbf{n}_{ab})(\mathbf{S}_b \cdot \mathbf{n}_{ab}) - (\mathbf{S}_a \cdot \mathbf{S}_a)]. \quad (\text{A.13})$$

The correction H_{SO}^{LO} accounts for spin-orbit coupling, $H_{S_a S_b}^{LO}$ accounts for coupling between the spin angular momenta of different objects and $H_{S_a^2}^{LO}$ is a correction accounting for gravitational effects caused by deformations in the objects due to their spin.

Appendix B

Orbital Elements Definitions

In this work we specify our initial conditions in terms of Keplerian orbital elements. Orbital elements allow us to specify the initial conditions of a binary in a way that makes information of the shape, size, and orientation of the orbit apparent. The orbits for inner and outer binaries are specified in terms of their minor radius a , eccentricity e , inclination i , longitude of the ascending node Ω , argument of periastron ω , and mean anomaly M . Several of these orbital elements are depicted in Fig. B.1. Orbital elements describe a binary in an elliptical orbit. While the orbits in our post-Newtonian simulations are not exactly elliptical, we find orbital elements are still the most useful way to specify our initial conditions. The inclination i is the angle the orbit makes with respect to a reference plane. The longitude of the ascending node Ω is the angle the orbit makes about an axis perpendicular to the reference plane with respect to some reference direction. Orbital nodes are the points where the orbit intersects the reference plane. The argument of periastron ω is the angle the major axis of the orbit makes about an axis perpendicular to the orbital plane, measured with respect to an orbital node. The true anomaly f is the angle the orbiting bodies make with respect to an orbital node. The mean anomaly M is calculated from the true anomaly f and eccentricity e

$$M = \arctan\left(\frac{\sqrt{1-e^2} \sin f}{e + \cos f}\right) - \frac{e\sqrt{1-e^2} \sin f}{1 + e \cos f}. \quad (\text{B.1})$$

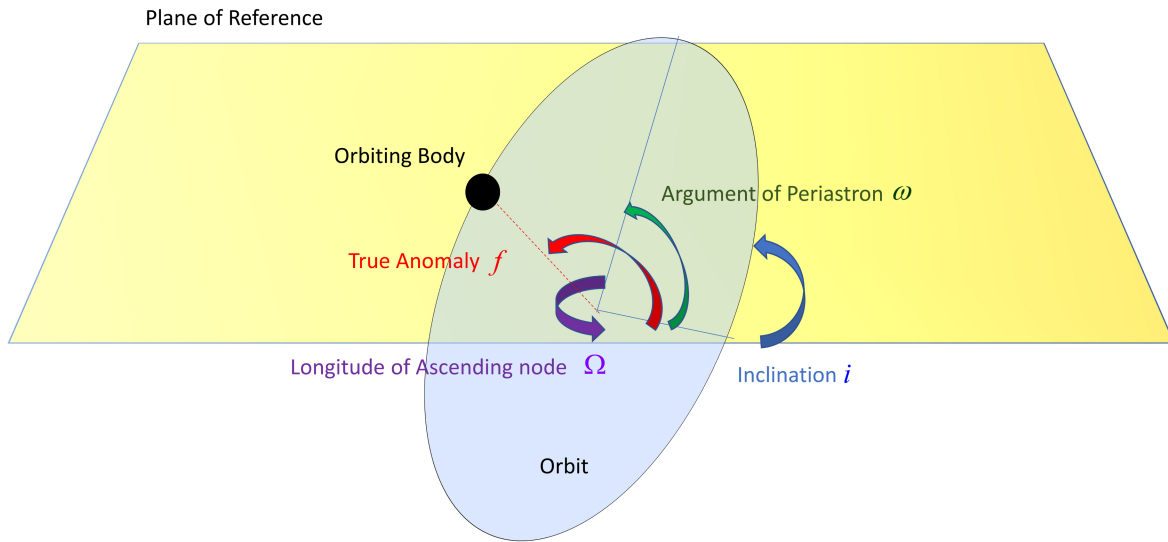


Fig. B.1 Depiction of Keplerian orbital elements

Conversion from Orbital Elements to Cartesian Coordinates

We specify our initial conditions in terms of orbital elements and then convert to Cartesian coordinates for our simulations. Here we discuss the process for converting from orbital elements to Cartesian coordinates. First, we calculate the eccentric anomaly u from the mean anomaly M by solving the following equation using Newton's method

$$M = u - e \sin u \quad (\text{B.2})$$

The true anomaly f is then calculated using

$$f = \arctan \left(\frac{\sin(u)\sqrt{1-e^2}}{\cos u - e} \right). \quad (\text{B.3})$$

We then calculate the polar coordinates of the orbit using

$$r = \frac{a(1-e^2)}{1-e \cos f} \quad (\text{B.4})$$

$$\phi = \Omega + \arctan[\tan(\omega + f) \cos i] \quad (\text{B.5})$$

$$\theta = \arccos[\sin(\omega + f) \sin i]. \quad (\text{B.6})$$

We then calculate the velocity of an orbiting body using

$$\dot{r} = g_r \dot{f} \quad (\text{B.7})$$

$$\dot{\theta} = g_\theta \dot{f} \quad (\text{B.8})$$

$$\dot{\phi} = g_\phi \dot{f}, \quad (\text{B.9})$$

where g_r , g_θ , g_ϕ , and \dot{f} are given by

$$g_r = \frac{a(1-e^2)e \sin f}{(1+e \cos f)^2} \quad (\text{B.10})$$

$$g_\theta = -\frac{1}{\sin \theta} \cos(\omega + f) \sin i \quad (\text{B.11})$$

$$g_\phi = \cos^2(\phi - \Omega) \frac{\cos i}{\cos^2(\omega + f)} \quad (\text{B.12})$$

$$\dot{f} = \sqrt{Gm' \left(\frac{2}{r} - \frac{1}{a} \right) \frac{1}{g_r^2 + (rg_\theta)^2 + (r \sin \theta g_\phi)^2}}, \quad (\text{B.13})$$

where m' is the total mass of the binary. For the inner binary $m' = m_1 + m_2$ and for the outer binary $m' = m_1 + m_2 + m_3$. We then convert these spherical coordinates in the one-body frame to Cartesian coordinates in the three-body frame.

Converting Cartesian Coordinates to Orbital Elements

After solving the post-Newtonian equations in cartesian coordinates we convert back to orbital elements. The semimajor axis a is calculated

$$a = -\frac{Gm'}{2E}, \quad (\text{B.14})$$

where m' is the total mass of the binary and E is the Newtonian energy per mass given by

$$E = \frac{1}{2}v^2 - \frac{Gm'}{r}, \quad (\text{B.15})$$

where v and r are the orbital velocity and position. The inclination i , eccentricity e , and ascending node Ω are given below

$$i = \arccos\left(\frac{(\mathbf{r} \times \mathbf{v})_z}{|\mathbf{r} \times \mathbf{v}|}\right) \quad (\text{B.16})$$

$$e = \sqrt{1 - \frac{|\mathbf{r} \times \mathbf{v}|}{aGm'}} \quad (\text{B.17})$$

$$\Omega = \arccos\left(\frac{(\mathbf{n} \times (\mathbf{r} \times \mathbf{v}))_x}{|\mathbf{n} \times (\mathbf{r} \times \mathbf{v})|}\right). \quad (\text{B.18})$$

Subscripts are used to denote vector components and \mathbf{n} is the unit vector perpendicular to the x-y plane. The argument of periastron ω is obtained as follows. First, the true anomaly f is given by

$$f = \arccos\left(\frac{a(1-e^2)-r}{er}\right) \quad (\text{B.19})$$

The angle from the ascending node θ is calculated

$$\theta = \arccos\left(\frac{x \cos \Omega + y \sin \Omega}{r}\right). \quad (\text{B.20})$$

The argument of periastron is

$$\omega = \theta - f. \quad (\text{B.21})$$

Index

adaptive step sizes 17
black hole 11-13, 12, 31-37
eccentricity 10, 24-26, 29-37, 45
general relativity 9, 14, 36
geometric units 17
gravitational waves 11-13, 33-35
Hamiltonian 14, 38-41
inclination 10, 42-46
initial conditions 16
integration methods 17
Kozai mechanism 10, 24-37
Marylou 17
orbital angular momentum 11
perturbation 14, 38-41
Post-Newtonian 14
spin angular momentum 11, 17, 27-28

Bibliography

- [1] J. Barrow-Green, Mathematical Society, *Isis* **89**, 345 (1998).
- [2] S. M. Ransom, I. H. Stairs, A. M. Archibald, J. W. Hessels, D. L. Kaplan, M. H. van Kerkwijk, J. Boyles, A. T. Deller, S. Chatterjee, A. Schechtman-Rook, A. Berndsen, R. S. Lynch, D. R. Lorimer, C. Karako-Argaman, V. M. Kaspi, V. I. Kondratiev, M. A. McLaughlin, J. van Leeuwen, R. Rosen, M. S. Roberts, and K. Stovall, *Nature* **505**, 520 (2014).
- [3] J. H. VanLandingham, M. C. Miller, D. P. Hamilton, and D. C. Richardson, *The Astrophysical Journal* **828**, 77 (2016).
- [4] O. Blaes, M. H. Lee, and A. Socrates, *The Astrophysical Journal* **578**, 775 (2002).
- [5] H. Suzuki, P. Gupta, H. Okawa, and K.-ichi Maeda, *Monthly Notices of the Royal Astronomical Society* **500**, 1645 (2020).
- [6] J. Abedi and N. Afshordi, *Journal of Cosmology and Astroparticle Physics* **2019**, 010 (2019).
- [7] J. J. Eldridge and E. R. Stanway, *Monthly Notices of the Royal Astronomical Society* **462**, 3302 (2016).
- [8] G. Fragione, A. Loeb, and F. A. Rasio, *The Astrophysical Journal* **902**, (2020).
- [9] S. Banerjee, *Monthly Notices of the Royal Astronomical Society* **500**, 3002 (2020).
- [10] O. D. Elbert, J. S. Bullock, and M. Kaplinghat, *Monthly Notices of the Royal Astronomical Society* **473**, 1186 (2017).
- [11] M. Hartl and A. Buonanno, *Physical Review D* **71**, (2005).
- [12] S. Isoyama, R. Sturani, and H. Nakano, *Handbook of Gravitational Wave Astronomy 1* (2021).
- [13] G. Schäfer and P. Jaranowski, *Living Reviews in Relativity* **21**, (2018).
- [14] H. Tagoshi, A. Ohashi, and B. J. Owen, *Physical Review D* **63**, (2001).
- [15] B. Ireland, O. Birnholtz, H. Nakano, E. West, and M. Campanelli, *Physical Review D* **100**, (2019).

[16] S. Tanay, L. C. Stein, and J. T. Gálvez Gherzi, *Physical Review D* **103**, (2021).

[17] C. Lubich, B. Walther, and B. Brügmann, *Physical Review D* **81**, (2010).